Similarity equation in non-axisymmetric lamellar eutectic growth

1992 J. Phys. A: Math. Gen. 25 3213

(http://iopscience.iop.org/0305-4470/25/11/027)

J. Phys. A: Math. Gen. 25 (1992) 3213–3237. Printed in the UK

Similarity equation in non-axisymmetric lamellar eutectic growth

K Kassner† and C Misbah‡§

† Institut für Festkörperforschung des Forschungszentrums Jülich, W-517 Jülich, Federal Republic of Germany

‡ Groupe de Physique des Solides, Université Paris VII et Paris VI, Associé au CNRS, Place Jussieu, 75005 Paris, France

Received 8 August 1991

Abstract. We extend our previous derivation of similarity laws in directional solidification of eutectics to general non-axisymmetric growth patterns. This involves mathematical subtleties which are not encountered in the symmetric case. The result explains our observation that numerical solutions describing tilted eutectic growth share the basic similarity property of axisymmetric solutions. We find additional scaling relations of the form $\lambda \sim V^{-1/2} g(G/V)$, e.g. for the wavelength λ of a tilted pattern at fixed tilt angle ϕ (V is the pulling velocity, G the temperature gradient). Discussing the question of universality of the scaling function g for different distinguished wavelengths, we are led to the prediction that the transition to a parity-broken state takes place at roughly twice the selected wavelength of the symmetric pattern for sufficiently large velocities and that the ratio of these wavelengths increases with decreasing velocity.

1. Introduction

When thin samples of eutectic alloys are directionally solidified, the generic growth mode of non-faceted systems is (in a certain velocity and concentration range) the formation of a periodic array of alternating lamellae of the two solid phases α and β. The lamellae are oriented (anti)parallel to the pulling direction. Much experimental and some theoretical work has been devoted to this type of lamellar growth. A review of the former has been given by Lesoult [1]. The origins of the latter date back to the 1940s [2, 3], and a decisive step forward was taken by Jackson and Hunt [4]. Their analysis indicates that steady-state growth should exist in a wide (even unbounded) range of wavelengths. In experiments, however, the dispersion of lamellar spacings is so small for given external constraints that even the selection of a unique wavelength seems likely. Whether this selection is an intrinsic system property or rather depends on experimental protocols, is a fascinating unanswered question. A heuristic criterion, already given in [4] (and earlier), identifies the operating point of lamellar growth with the wavelength at which the average undercooling of the solid–liquid interface is minimum. Later, it was attempted [5, 6] to justify this criterion on the basis of a stability calculation showing that the minimum undercooling point coincides with the point of marginal stability of the system. However, this analysis involved simplifying

§ Present address: Institut Laue-Langevin, BP 156X, 38042 Grenoble, France.

0305-4470/92/113213+25$04.50

assumptions which were recently shown [7] to be unjustified, at least in the limit of the large thermal gradient to which the latter calculation pertains. This more general stability analysis showed that growth patterns are stable in a neighbourhood of the minimum undercooling point.

A full diffusive instability treatment at arbitrary thermal gradient, along the lines of similar work on directional solidification of dilute alloys [8], should clearly be performed to complete the picture [9]. Moreover, while the minimum undercooling criterion seems to work well in general, there has been some experimental evidence that it may not be exactly correct [10]. In view of this unclear situation, it is interesting that one can make exact statements about scaling laws for the wavelength selection without knowing the selection mechanism. Recently, we have been able to derive, from the full boundary integral equation pertinent to eutectic growth, a similarity equation which is valid in the experimentally relevant range of small Péclet numbers [11, 12]. We showed that the dynamical properties of the system depend on two parameters only, $\sigma = d_0 l/\lambda^2$ and $\chi = l/l_T$, where λ is the lamellar spacing, l the diffusion length and d_0 and l_T are capillary and thermal lengths respectively. This implies that the selected wavelength scales as $\lambda \sim V^{-1/2} f(l/l_T)$, wherein V is the pulling velocity, from which $\lambda \sim V^{-1/2}$ follows *exactly*, if the ratio l/l_T (i.e. the ratio of thermal gradient and velocity) is kept constant. Assuming the minimum undercooling criterion to hold, we furthermore determined the scaling function f numerically and showed that at constant thermal gradient $\lambda \sim V^{-\beta}$, where $\beta \approx \frac{1}{2}$ at large velocity and β decreases with decreasing velocity, in agreement with experiments [1].

Another recent development is the experimental observation [13] of small domains of *tilted* lamellae after application of a positive velocity jump. These domains, which move transversely along the growth front, were suggested to be localized inclusions of a new antisymmetric state [14]. The original untilted state is symmetric with respect to the central axes of both the α and β phases. Thus the appearance of tilted states is a parity-breaking transition inasmuch as the equations of motion are also symmetric under reflection at the symmetry axes. We have shown recently [15] that indeed the fully isotropic model of eutectic growth supports solutions with broken parity symmetry. In addition, we determined that the bifurcation to these non-axisymmetric states is of standard supercritical type, which led us to predict that on application of a sufficiently large velocity jump (by a factor of 4 or so), the tilted domains would invade all the space of the sample [16]. This prediction has meanwhile been confirmed experimentally [17].

We found numerically [11, 12] that similarity holds for tilted solutions as well as for untilted ones. However, our previous derivation of the similarity equation critically depended on the axisymmetry of the pattern. Without this axisymmetry, a certain integral would have diverged when its integrand was replaced by its small Péclet number limit.

The purpose of the present paper is to show how this problem can be resolved, to derive the similarity equation for tilted, i.e. non-axisymmetric patterns, and to discuss its physical consequences. The derivation involves some mathematical subtleties rarely encountered in physics where things tend either to converge uniformly or to need renormalization. Here, none of the two cases applies. Nevertheless, the limit $P \to 0$ (P: Péclet number) of the boundary integral equation can be performed exactly.

In the next section we give the model equations and reduce them to a form which is suitable for similarity considerations. Section 3 contains the derivation of the sim-

ilarity equation, with some of the mathematical details relegated to the appendices. In section 4, we demonstrate the similarity properties explicitly for the growth morphology as well as the average undercooling and the tilt angle. Section 5 summarizes a few conclusions.

2. The model

As usual, we assume that thermal transport processes are much faster than chemical diffusion, with latent heat production being negligible, and that thermal conductivities are the same in all three phases, i.e. heat diffusion proceeds symmetrically [18]. The first assumption allows us to decouple the thermal and chemical diffusion problems, the second renders the thermal problem trivial in the conventional directional solidification set-up [12]—the temperature profile is linear with a constant temperature gradient G. So we are left with the chemical problem. In order to describe its basic features we give the phase diagram in figure 1. Assuming vanishing (chemical) diffusivity in the solid(s), i.e. considering the one-sided model, we can reduce the description to a single concentration $c(\boldsymbol{r},t)$ in the liquid, for which we choose that of the major component of the β phase (see figure 1). After introduction of a dimensionless concentration field $u(\boldsymbol{r},t) = (c(\boldsymbol{r},t) - c_e)/\Delta c$—for the definitions of c_e and Δc see the figure—the equation of motion for stationary growth reads, in the frame of reference which is attached to the interface:

$$\nabla^2 u(\boldsymbol{r}) + \frac{2}{l}\left(\frac{\partial}{\partial z} + \tan\phi\frac{\partial}{\partial x}\right) u(\boldsymbol{r}) = 0\,. \tag{2.1}$$

Herein, $l = 2D/V$ is the diffusion length; D the diffusion coefficient in the liquid. In writing the equation, we have taken into account the experimental fact that patterns with broken parity drift laterally with constant velocity $V\tan\phi$. The tilt angle ϕ, *a*

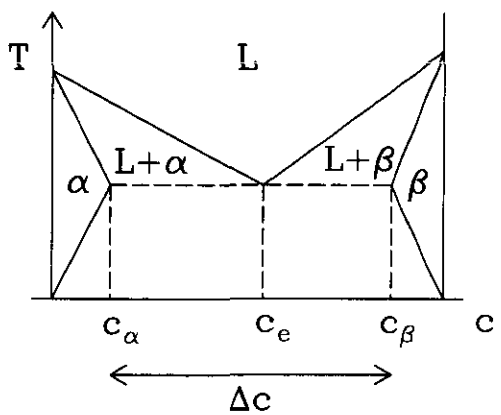

Figure 1. Generic phase diagram of eutectics. T is the temperature, c the concentration of one component. The regions L, α, and β correspond to one-phase equilibrium states of the liquid, the solid α and the solid β phases respectively. $L+\alpha$ and $L+\beta$ are of two-phase equilibrium between the liquid and one solid phase; the true concentrations of the two phases are given by the liquidus and solidus lines (full lines) delimiting these regions. c_e, c_α and c_β denote the equilibrium concentrations of the liquid and the two solid phases at the triple or eutectic point; Δc is the miscibility gap: $\Delta c = c_\beta - c_\alpha$.

priori unknown, obtains from a solution of (2.1) with all boundary conditions, and it has been shown [15, 16] that there exists only a discrete set of solutions for ϕ. When cast into the form of a boundary integral equation, the equation of motion of the system becomes

$$\int_{\Gamma_{sl}} d\Gamma'\, g(\boldsymbol{r},\boldsymbol{r}')\frac{\partial u}{\partial n'} = \int_{\Gamma_{sl}} d\Gamma'\, h(\boldsymbol{r},\boldsymbol{r}';\boldsymbol{n}')\,(u(\boldsymbol{r}')-u_\infty) \tag{2.2}$$

where $u_\infty = (c_\infty - c_e)/\Delta c$ is the reduced concentration at infinity (taken constant). The integration contour Γ_{sl} runs along the liquid–solid interface—see figure 2. We have restricted ourselves to 1D deformations, so $g(\boldsymbol{r},\boldsymbol{r}')$ is the 2D Green function (for natural boundary conditions) corresponding to the differential operator acting on $u(\boldsymbol{r})$ in (2.1). It is given by

$$g(\boldsymbol{r},\boldsymbol{r}') = \frac{1}{2\pi}\exp\left[-(\Delta\zeta + \Delta x\tan\phi)/l\right] K_0\left(\frac{\rho}{l\cos\phi}\right) \tag{2.3}$$

where $\boldsymbol{r} = (x,\zeta)$, $\boldsymbol{r}' = (x',\zeta')$, $\Delta x = x - x'$, $\Delta\zeta = \zeta - \zeta'$, and $\rho = \sqrt{\Delta x^2 + \Delta\zeta^2}$. Because $\boldsymbol{r}'$ is restricted to the interface, ζ' is a (not necessarily single-valued) function of x': $\zeta' = \zeta(x')$; K_0 is the modified Bessel function of zeroth order [19]. Finally, $h(\boldsymbol{r},\boldsymbol{r}';\boldsymbol{n}')$ is an expression involving the normal derivative of $g(\boldsymbol{r},\boldsymbol{r}')$:

$$h(\boldsymbol{r},\boldsymbol{r}';\boldsymbol{n}') = \frac{1}{2\pi l}\exp\left[-(\Delta\zeta + \Delta x\tan\phi)/l\right]\left\{-(n'_z + n'_x\tan\phi)K_0\left(\frac{\rho}{l\cos\phi}\right)\right.$$
$$\left. - \frac{\boldsymbol{n}'(\boldsymbol{r}'-\boldsymbol{r})}{\rho\cos\phi}K_1\left(\frac{\rho}{l\cos\phi}\right)\right\} - c_r\delta(\boldsymbol{r}-\boldsymbol{r}') \tag{2.4}$$

where $\boldsymbol{n}' = (n'_x, n'_z)$ is the normal vector at $\boldsymbol{r}'$ pointing from the solid into the liquid (see figure 2). K_1 is the modified Bessel function of first order. The δ function is 1D, i.e. it is defined via a contour integral, not (as usual) a (2D) volume integral. The prefactor c_r of the δ function is $\frac{1}{2}$ if the interface is smooth at $\boldsymbol{r}$; for more details see [20, 21].

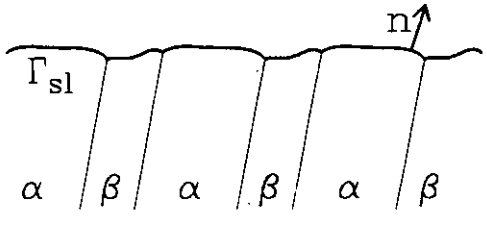

Figure 2. Definition of the contour of integration Γ_{sl} and the direction of the normal vector $\boldsymbol{n}$ on it.

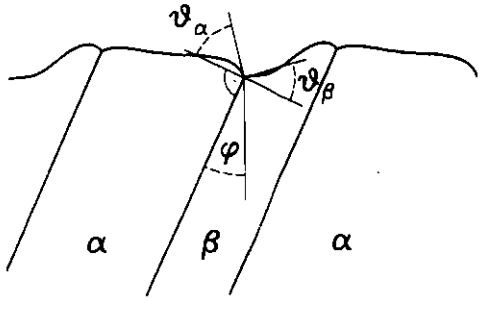

Figure 3. Definition of the contact angles ϑ_α, ϑ_β, and the tilt angle ϕ. Note that ϕ is counted positive for a tilt to the right, while ϑ_α and ϑ_β are always positive.

The physical boundary conditions of the problem are provided by the Gibbs–Thomson condition, the continuity equation and the mechanical equilibrium conditions at the triple points. Assuming that the interface kinetics are instantaneous on the time scale of the diffusion, we take the interface to be at local thermodynamic equilibrium, which means, in particular, that it is microscopically rough. Then the Gibbs–Thomson condition tells us that, at the interface,

$$u = \begin{cases} -\zeta/l_{\mathrm{T}}^{\alpha} - d_0^{\alpha}\kappa & \alpha \text{ phase} \\ \zeta/l_{\mathrm{T}}^{\beta} + d_0^{\beta}\kappa & \beta \text{ phase.} \end{cases} \tag{2.5}$$

In these equations, ζ is the z coordinate of the liquid–solid interface and κ its curvature, taken positive where the solid is convex; $l_{\mathrm{T}}^{\alpha/\beta}$ are the thermal lengths, given by $l_{\mathrm{T}}^{i} = m_i \Delta c/G$, where m_i $(i = \alpha, \beta)$ is the absolute value of the slope of the liquidus line describing coexistence of phase i and the liquid (figure 1); d_0^i are the capillary lengths: $d_0^i = \gamma_{il} T_{\mathrm{e}}/L_i m_i \Delta c$, where γ_{il} is the liquid–solid–i interface tension, T_{e} the temperature of three-phase equilibrium, and the L_i are effective latent heats per unit volume.†. All surface tensions are assumed to be isotropic.

Mass conservation for fluxes to and from the interface is written as the following continuity equations:

$$-D\frac{\partial u}{\partial n} = \begin{cases} [(1-k_\alpha)u + \delta]\, v_{\mathrm{n}} & \alpha \text{ phase} \\ [(1-k_\beta)u + \delta - 1]\, v_{\mathrm{n}} & \beta \text{ phase} \end{cases} \tag{2.6}$$

where $\delta = (c_{\mathrm{e}} - c_\alpha)/\Delta c$ is the reduced miscibility gap of the α phase, $1-\delta$ that of the β phase and k_α, k_β are the partition coefficients. For our 'linearized' phase diagram, these are simply the ratios of the constant slopes of the respective liquidus and solidus lines (figure 1)‡. The normal velocity v_{n} of a stationary tilted pattern is given by

$$v_{\mathrm{n}} = \frac{2D}{l}(n_z + \tan\phi\, n_x)\,. \tag{2.7}$$

Finally, imposing mechanical equilibrium at the triple points, we obtain

$$\begin{aligned} \gamma_{\alpha l}\sin(\vartheta_\alpha \mp \phi) + \gamma_{\beta l}\sin(\vartheta_\beta \pm \phi) &= \gamma_{\alpha\beta}\cos\phi \\ \gamma_{\alpha l}\cos(\vartheta_\alpha \mp \phi) - \gamma_{\beta l}\cos(\vartheta_\beta \pm \phi) &= \pm\gamma_{\alpha\beta}\sin\phi \end{aligned} \tag{2.8}$$

† The latent heats that enter the definition of the capillary lengths d_0^i are not exactly those of the α/liquid and β/liquid transitions, but effective quantities. This can be seen by following the derivation given in [22] for a quasi-azeotrope. There the effective heat of transition reduces to the latent heat only because the concentrations of the solid and liquid phases are equal at the azeotropic point (which is not the case for eutectics).

‡ Note that equations (2.6) are a simplification of the exact mass conservation equations for a non-dilute system. Indeed, the terms in square brackets must be understood as $\propto (c_{\mathrm{l}} - c_{si})$, $i = \alpha, \beta$. Thermodynamic equilibrium at the front imposes that (see [22]) $(c_{si} - c_i) = k_i(c_{\mathrm{l}} - c_{\mathrm{e}}) + d_0^{\mathrm{c}}\kappa$, where κ is the front curvature. The capillary length d_0^{c}, which vanishes for dilute alloys, turns out to be negligible for eutectics with small temperature gaps $(m_i \Delta c_i)$. This is the case for the CBr_4–C_2Cl_6 eutectic in which we are interested here. We should, however, keep in mind that there are some eutectics for which d_0^{c} is not small, especially due to a large temperature gap (e.g. Pb–Sn).

where ϑ_α and ϑ_β are the contact angles—see figure 3—and the upper signs hold for the triple point to the left, the lower ones for that to the right of the α phase. The contact angles are uniquely determined by the surface tensions. The pinning angles, which are measured from a baseline parallel to the x axis, then take on the values $\vartheta_\alpha \mp \phi$ and $\vartheta_\beta \pm \phi$ respectively.

Because the boundary conditions determine, in terms of $\zeta(x')$, both $u(\boldsymbol{r}')$ and $\partial u/\partial n'$ in (2.2), the integral equation—with $\boldsymbol{r}$ taken to the interface—constitutes a closed functional equation for the solidification front $\zeta(x)$– or the contour Γ_{sl}.

Since we wish to detect similarity properties of the pattern, including geometric similarity, we rewrite the integral equation and its boundary conditions in dimensionless form, with lengths measured in units of λ. The eutectic problem contains six length parameters, namely the periodicity λ of the pattern, the diffusion length l, two capillary lengths d_0^α and d_0^β and two thermal lengths l_T^α and l_T^β. For a given material, the ratio of the two capillary lengths and that of the thermal lengths is constant under most variations of the experimental conditions. This means that there are actually only four relevant (i.e. dynamically variable) length scales, which on introduction of dimensionless ratios reduce to three parameters, for which we choose $P = \lambda/l$ (the Péclet number), $\sigma = d_0^\alpha l/\lambda^2$, and $\chi = l/l_T^\alpha$. We will show by derivation of the similarity equation that for small P all system properties depend only on two parameters, i.e. P scales out of the equation.

Transforming equation (2.5) to length units of λ (replacing r with $r\lambda$, κ with κ/λ), we obtain

$$u = -P\epsilon(x)\left\{\chi\zeta(x) + \psi(x)\sigma\kappa(x)\right\} \equiv P\tilde{u}(x) \tag{2.9}$$

where

$$\epsilon(x) = \begin{cases} 1 & \alpha \text{ phase} \\ -l_T^\alpha/l_T^\beta & \beta \text{ phase} \end{cases} \tag{2.10}$$

and

$$\psi(x) = \begin{cases} 1 & \alpha \text{ phase} \\ l_T^\beta d_0^\beta / l_T^\alpha d_0^\alpha & \beta \text{ phase} \end{cases} \tag{2.11}$$

are piecewise constant functions. For definiteness, we choose the origin of the x axis to align with a triple point to the left of an α phase lamella, i.e. the x coordinate of the α–l interface runs between 0 and x_e, which is the abscissa of the triple point to the right of the lamella; the β–l interface belonging to the same periodicity unit then has $x \in [x_e, 1]$. Note that $\tilde{u}$ does not explicitly depend on P but on χ and σ only. Using $n_x = -\zeta_x n_z$, where $\zeta_x = \partial\zeta/\partial x$, we obtain the transformed continuity equation ($\partial/\partial n \to \lambda^{-1}\partial/\partial n$)

$$\frac{\partial u}{\partial n} = -\left\{[1 - k(x)]P\tilde{u}(x) + H(x)\right\} 2Pn_z(1 - \zeta_x \tan\phi) \tag{2.12}$$

with

$$k(x) = \begin{cases} k_\alpha & \alpha \text{ phase} \\ k_\beta & \beta \text{ phase} \end{cases} \tag{2.13}$$

and

$$H(x) = \begin{cases} \delta & \alpha \text{ phase} \\ \delta - 1 & \beta \text{ phase.} \end{cases} \tag{2.14}$$

Inserting (2.9) and (2.12) into the integral equation (2.2) and employing $\mathrm{d}x' = \mathrm{d}\Gamma' n_z'$, we arrive at the following form of the integral equation:

$$\begin{aligned} \frac{\tilde{u}(x)}{2} = \frac{u_\infty}{P} &+ \frac{1}{2\pi}\int_{-\infty}^{\infty} \mathrm{d}x' \exp\left[-P(\Delta\zeta + \Delta x \tan\phi)\right](1 - \zeta_{x'}\tan\phi) \\ &\times \left[2H(x') + (1 - 2k(x'))\, P\tilde{u}(x')\right] K_0\left(P\frac{\rho}{\cos\phi}\right) \\ &+ \frac{1}{2\pi}\int_{-\infty}^{\infty} \mathrm{d}x' \exp\left[-P(\Delta\zeta + \Delta x\tan\phi)\right]\frac{\Delta\zeta - \Delta x\zeta_{x'}}{\rho\cos\phi}\, P\tilde{u}(x') \\ &\times K_1\left(P\frac{\rho}{\cos\phi}\right). \end{aligned} \tag{2.15}$$

In order to move u_∞ in front of the integral terms, we have made use of the sum rule

$$\int_{\Gamma_\alpha} \mathrm{d}\Gamma'\, h(\boldsymbol{r}, \boldsymbol{r}'; \boldsymbol{n}') = -1 \tag{2.16}$$

which has been derived in various contexts [16, 23].

Equation (2.15) is our starting-point for the derivation of the similarity equation.

3. The similarity equation

To obtain the similarity equation we must perform the limit $P \to 0$ of the integral equation (2.15). This limit is not uniform which makes the task non-trivial. We consider the two integrals in (2.15) separately:

$$\frac{\tilde{u}(x)}{2} = \frac{u_\infty}{P} + I_1(P) + I_2(P) \tag{3.1}$$

$$\begin{aligned} I_1(P) = \frac{1}{2\pi}\int_{-\infty}^{\infty} &\mathrm{d}y\, \mathrm{e}^{-P\Delta\zeta}\, \mathrm{e}^{-\hat{P}y}(1 + \zeta_y \tan\phi) K_0(\tilde{P}\rho) \\ &\times \left[2H(x-y) + (1 - 2k(x-y))\, P\tilde{u}(x-y)\right] \end{aligned} \tag{3.2}$$

$$I_2(P) = \frac{1}{2\pi}\int_{-\infty}^{\infty} \mathrm{d}y\, \mathrm{e}^{-P\Delta\zeta}\, \mathrm{e}^{-\hat{P}y}\frac{\Delta\zeta + y\zeta_y}{\rho}\tilde{P}\tilde{u}(x-y) K_1(\tilde{P}\rho). \tag{3.3}$$

In these equations, we have introduced a new integration variable, $y = x - x'$, and the abbreviations $\tilde{P} = P/\cos\phi$ and $\hat{P} = P\tan\phi$. Obviously, $\tilde{P}^2 - \hat{P}^2 = P^2$ and $\tilde{P} > \hat{P}$. This inequality ensures the convergence of both integrals even at the lower integration bound where $\mathrm{e}^{-\hat{P}y}$ blows up, because the asymptotic behaviour of the Bessel functions for large arguments ($K_\nu(\tilde{P}\rho) \sim \sqrt{\pi/2\tilde{P}\rho}\, \mathrm{e}^{-\tilde{P}\rho}$) [19] guarantees

an exponentially decaying integrand ($\rho = \sqrt{y^2 + \Delta\zeta^2} > |y|$). Despite the singular behaviour of K_1 at $y = 0$ ($K_1(\tilde{P}\rho) \sim 1/\tilde{P}\rho$) [19], the integral I_2 is convergent there because

$$\frac{\Delta\zeta + y\zeta_y}{\rho^2} \xrightarrow[y\to 0]{} \frac{\zeta_{yy}(x)}{2\left[1 + \zeta_y^2(x)\right]} \tag{3.4}$$

which is finite. Note that if x is the coordinate of a triple point, the right-hand side expression has to be replaced with an appropriate left-sided or right-sided limit, which means that the integrand has a jump discontinuity, i.e. it remains integrable.

These considerations suggest that $\lim_{P\to 0} I_2$ might be calculated by taking the limit inside the integral, a procedure which would be correct if the integral were uniformly convergent as a function of P. However, this is not the case. The most slowly decaying term of the $P \to 0$ limit of the integrand is

$$\frac{y\zeta_y\tilde{u}(x-y)}{\rho^2} \underset{|y|\gg 1}{\sim} \pm\frac{\zeta_y\tilde{u}(x-y)}{|y|}. \tag{3.5}$$

The integral of this quantity diverges, in general, at the lower and upper integration bounds. In [12] we showed that it is convergent for axisymmetric profiles, because then $\zeta_y\tilde{u}$ is an odd function with respect to the symmetry axes, whose integral over one period vanishes. In that case I_2 could indeed be shown to converge uniformly [12]. Note that by reinterpreting the formal expression $I_2(0)$ (meaning I_2 with the integrand replaced by its $P \to 0$ limit) as a principal value integral, $\int_{-\infty}^{\infty} \mathrm{d}y \ldots \to \lim_{R\to\infty} \int_{-R}^{R} \mathrm{d}y \ldots$, convergence is re-established for arbitrary profiles $\zeta(x-y)$, because the dangerous contributions of the even part of $\zeta_y\tilde{u}$ at the lower and upper boundaries cancel each other out. Nevertheless, this does not reinstate uniform convergence, i.e. for non-axisymmetric profiles we have $\lim_{P\to 0} I_2(P) \neq I_2(0)$.

In order actually to calculate the limit we have to split the integral into uniformly convergent parts and a part which can be computed explicitly. First, we introduce a few abbreviations:

$$F_P(y) = \frac{1}{2\pi}\,\mathrm{e}^{-P\Delta\zeta}\ \Delta\zeta\ \tilde{u}(x-y) \tag{3.6}$$

$$g_P(y) = \frac{1}{2\pi}\,\mathrm{e}^{-P\Delta\zeta}\ \zeta_y\ \tilde{u}(x-y) \tag{3.7}$$

$$\bar{g}_P \equiv \langle g_P(y)\rangle = \int_0^1 \mathrm{d}y\, g_P(y). \tag{3.8}$$

Both functions are periodic with period 1. We then have

$$I_2 = \int_{-\infty}^{\infty} \mathrm{d}y\,[F_P(y) + y g_P(y)]\ \tilde{P}\ \mathrm{e}^{-\hat{P}y}\,\frac{K_1(\tilde{P}\rho)}{\rho} \equiv I_{2a} + I_{2b} + I_{2c} \tag{3.9}$$

with

$$I_{2a} = \int_{-\infty}^{\infty} \mathrm{d}y\,[F_P(y) + y(g_P(y) - \bar{g}_P)]\ \tilde{P}\ \mathrm{e}^{-\hat{P}y}\,\frac{K_1(\tilde{P}\rho)}{\rho} \tag{3.10}$$

$$I_{2b} = \int_{-\infty}^{\infty} \mathrm{d}y\, y\bar{g}_P\tilde{P}\ \mathrm{e}^{-\hat{P}y}\left(\frac{K_1(\tilde{P}\rho)}{\rho} - \frac{K_1(\tilde{P}|y|)}{|y|}\right) \tag{3.11}$$

$$I_{2c} = \int_{-\infty}^{\infty} \mathrm{d}y\,\bar{g}_P\ \tilde{P}\ \mathrm{e}^{-\hat{P}y}\,\frac{yK_1(\tilde{P}|y|)}{|y|} \tag{3.12}$$

where we have to take all integrals as principal value integrals, because otherwise the $\bar{g}_P$ terms diverge at $y = 0$. To be precise, we defined $\oint_{-\infty}^{\infty} \mathrm{d}y \cdots = \lim_{\epsilon \to 0+} (\int_{-\infty}^{-\epsilon} + \int_{\epsilon}^{\infty}) \mathrm{d}y \cdots$.

In appendix A we show that both I_{2a} and I_{2b} are uniformly convergent which leads to

$$\lim_{P \to 0} I_{2a} = I_{2a}(0) = \oint_{-\infty}^{\infty} \mathrm{d}y \, [F_0(y) + y(g_0(y) - \bar{g}_0)] \frac{1}{\rho^2} \tag{3.13}$$

$$\lim_{P \to 0} I_{2b} = I_{2b}(0) = \oint_{-\infty}^{\infty} \mathrm{d}y \, y \bar{g}_0 \left(\frac{1}{\rho^2} - \frac{1}{y^2} \right) \tag{3.14}$$

where the small argument expansion of K_1 has been used. Furthermore, we prove that

$$\oint_{-\infty}^{\infty} \mathrm{d}x \, \mathrm{e}^{bx} \frac{x K_1(\alpha |x|)}{|x|} = \frac{\pi b}{\alpha \sqrt{\alpha^2 - b^2}} \tag{3.15}$$

which immediately yields

$$I_{2c} = \bar{g}_P \tilde{P} \frac{-\pi \hat{P}}{\tilde{P} P} = -\pi \tan \phi \, \bar{g}_P \tag{3.16}$$

and hence

$$\lim_{P \to 0} I_{2c}(P) = -\pi \tan \phi \, \bar{g}_0 = -\frac{1}{2} \tan \phi \int_0^1 \mathrm{d}y \, \zeta_y \, \tilde{u}(x - y). \tag{3.17}$$

Adding all three terms together, we arrive at

$$\lim_{P \to 0} I_2(P) = \oint_{-\infty}^{\infty} \mathrm{d}y \left\{ \frac{1}{2\pi} \frac{\Delta\zeta + y\zeta_y}{\rho^2} \tilde{u}(x - y) - \frac{\bar{g}_0}{y} \right\} - \pi \tan \phi \, \bar{g}_0. \tag{3.18}$$

Now the second term in the integral is an odd function, which only serves to cancel the divergence of the first term at large values of $|y|$. On reinterpretation of the full integral as a different principal value integral we can simply omit that term. Defining $\oint_{-\infty}^{\infty} \mathrm{d}y \cdots = \lim_{R \to \infty} \int_{-R}^{R} \mathrm{d}y \cdots$ we obtain

$$\begin{aligned} \lim_{P \to 0} I_2(P) &= \text{`}I_2(0)\text{'} - \pi \tan \phi \, \bar{g}_0 \\ &= \frac{1}{2\pi} \oint_{-\infty}^{\infty} \mathrm{d}y \, \frac{\Delta\zeta + y\zeta_y}{\rho^2} \tilde{u}(x - y) - \frac{1}{2} \tan \phi \int_0^1 \mathrm{d}y \, \zeta_y \tilde{u}(x - y). \end{aligned} \tag{3.19}$$

Next we consider I_1. We introduce new abbreviations

$$G(y) = (1 + \zeta_y \tan \phi)(1 - 2k(x - y))\tilde{u}(x - y) \tag{3.20}$$

$$\tilde{H}(y) = (1 + \zeta_y \tan \phi) H(x - y) \tag{3.21}$$

$$L_P(y) = (\mathrm{e}^{-P\Delta\zeta} - 1)\,[PG(y) + 2\tilde{H}(y)]. \tag{3.22}$$

All of these functions are periodic with period 1. They depend parametrically on x, actually being functions of $x - y$, but only L_P depends on P explicitly. Again we split off a uniformly convergent part by writing

$$I_1(P) = I_{1a}(P) + I_{1b}(P) + I_{1c}(P) \tag{3.23}$$

$$I_{1a} = \frac{1}{2\pi}\int_{-\infty}^{\infty} \mathrm{d}y\, \mathrm{e}^{-P\Delta\zeta}\,[PG(y) + 2\tilde{H}(y)]\mathrm{e}^{-\hat{P}y}(K_0(\tilde{P}\rho) - K_0(\tilde{P}|y|)) \tag{3.24}$$

$$I_{1b} = \frac{1}{2\pi}\int_{-\infty}^{\infty} \mathrm{d}y\, L_P(y)\mathrm{e}^{-\hat{P}y}K_0(\tilde{P}|y|) \tag{3.25}$$

$$I_{1c} = \frac{1}{2\pi}\int_{-\infty}^{\infty} \mathrm{d}y\,[PG(y) + 2\tilde{H}(y)]\mathrm{e}^{-\hat{P}y}K_0(\tilde{P}|y|). \tag{3.26}$$

The proof that I_{1a} is uniformly convergent is completely analogous to that given for I_{2b} in appendix A. This allows us immediately to write down the limit

$$\lim_{P\to 0} I_{1a}(P) = I_{1a}(0) = \frac{1}{\pi}\int_{-\infty}^{\infty} \mathrm{d}y\,(1 + \zeta_y \tan\phi)H(x-y)\ln\frac{|y|}{\rho} \tag{3.27}$$

where the logarithm comes from the small argument expansion of K_0 [19].

Here, I_{1b} and I_{1c} are evaluated by expansion of the periodic functions G, $\tilde{H}$ and L_P into Fourier series:

$$G(y) = \sum_{n=-\infty}^{\infty} b_n \mathrm{e}^{-\mathrm{i}2\pi n y} \tag{3.28}$$

$$\tilde{H}(y) = \sum_{n=-\infty}^{\infty} c_n \mathrm{e}^{-\mathrm{i}2\pi n y} \tag{3.29}$$

$$L_P(y) = \sum_{n=-\infty}^{\infty} d_n(P)\mathrm{e}^{-\mathrm{i}2\pi n y}. \tag{3.30}$$

The basic integral needed is equation (A.14) of appendix A:

$$\begin{aligned}\int_{-\infty}^{\infty} \mathrm{d}y\, \exp[-(\hat{P} + 2\mathrm{i}\pi n)y]K_0(\tilde{P}|y|) &= \frac{\pi}{(\tilde{P}^2 - (\hat{P} + 2\mathrm{i}\pi n)^2)^{1/2}} \\ &= \frac{\pi}{(P^2 - 2\mathrm{i}\pi n\hat{P} + 4\pi^2 n^2)^{1/2}} \\ &\underset{P\to 0}{\sim} \begin{cases} \pi/P & \text{for } n = 0 \\ 1/2|n| & \text{for } n \neq 0. \end{cases}\end{aligned} \tag{3.31}$$

The integrals are sufficiently well behaved to allow the commutation of the order of integration and the summation on n. Furthermore, the limit $P \to 0$ may be performed term by term on the resulting sums (this is easy to see for the sums

containing the coefficients b_n and c_n and requires a little more effort for $d_n(P)$). We then arrive at

$$\lim_{P\to 0} I_{1b}(P) = \lim_{P\to 0} \frac{d_0(P)}{2P} \tag{3.32}$$

$$\lim_{P\to 0} \left(I_{1c}(P) - \frac{c_0}{P}\right) = \frac{1}{2}b_0 + \sum_{\substack{n=-\infty \\ n\neq 0}}^{\infty} \frac{c_n}{2\pi|n|} \tag{3.33}$$

and all that remains to be done is the evaluation of the Fourier coefficients plus a discussion of the apparently divergent terms of order $1/P$ in (3.1) and (3.33).

We have

$$\lim_{P\to 0} \frac{d_0}{2P} = \lim_{P\to 0} \int_0^1 \mathrm{d}y \, \frac{\mathrm{e}^{-P\Delta\zeta} - 1}{2P} [PG(y) + 2\tilde{H}(y)]$$

$$= -\int_0^1 \mathrm{d}y \, \Delta\zeta(1 + \zeta_y \tan\phi) H(x - y) \tag{3.34}$$

$$b_0 = \int_0^1 \mathrm{d}y \, (1 + \zeta_y \tan\phi)(1 - 2k(x - y))\tilde{u}(x - y) \tag{3.35}$$

$$c_0 = \int_0^1 \mathrm{d}y \, (1 + \zeta_y \tan\phi) H(x - y)$$

$$= \int_0^{x_e} \mathrm{d}x' \, (1 - \zeta_{x'} \tan\phi) \, \delta + \int_{x_e}^1 \mathrm{d}x' \, (1 - \zeta_{x'} \tan\phi)(\delta - 1)$$

$$= x_e + \delta - 1 + \tan\phi \, [\zeta(0) - \zeta(x_e)]. \tag{3.36}$$

In the last calculation we have switched back to a description in terms of $x' = x - y$, using the periodicity of the integrand to keep the integration bounds at 0 and 1 as well as to evaluate the integral. It can now be shown (see appendix B) that for tilted growth the volume fraction η of the α phase is (in our reduced units) given by

$$\eta = x_e + \tan\phi \, [\zeta(0) - \zeta(x_e)] \tag{3.37}$$

and hence

$$c_0 = \delta + \eta - 1 \tag{3.38}$$

formally the same as in the axisymmetric case, but with a quite different definition of η in terms of the geometric quantities x_e and $\zeta(x_e)$. We proceed with the calculation of the sum on n in (3.33):

$$\sum_{\substack{n=-\infty \\ n\neq 0}}^{\infty} \frac{c_n}{2\pi|n|} = \sum_{\substack{n=-\infty \\ n\neq 0}}^{\infty} \int_0^1 \mathrm{d}y \, (1 + \zeta_y \tan\phi) H(x - y) \frac{\mathrm{e}^{2i\pi ny}}{2\pi|n|}$$

$$= \int_0^1 \mathrm{d}y \, (1 + \zeta_y \tan\phi) H(x - y) \sum_{n=1}^{\infty} \frac{\cos 2n\pi y}{\pi n}$$

$$= -\frac{1}{\pi} \int_0^1 \mathrm{d}y \, (1 + \zeta_y \tan\phi) H(x - y) \ln(2\,|\sin \pi y|) \tag{3.39}$$

where we have used $\sum_{n=1}^{\infty} \cos nx/n = -\ln(2\sin x/2)$, for $x \in (0, 2\pi)$ (no 24, p 666 in [24]). Note that the logarithmic divergences at $y = 0$ and $y = 1$ are integrable and that we introduced the absolute value to keep the periodicity of the integrand equal to 1, allowing later a shift of the integration boundaries (to arrive at equation (3.43)). In fact, there is a different, more familiar representation for the first term (not containing ζ_y) of the integral, allowing its explicit evaluation. This leads to

$$\sum_{\substack{n=-\infty \\ n\neq 0}}^{\infty} \frac{c_n}{2\pi|n|} = \sum_{n=1}^{\infty} \frac{\sin n\pi x_e}{(n\pi)^2} \cos 2n\pi\left(x - \frac{x_e}{2}\right)$$

$$- \frac{1}{\pi} \tan\phi \int_0^1 \mathrm{d}y\, \zeta_y H(x-y) \ln(2|\sin \pi y|). \tag{3.40}$$

Finally, we collect the terms which are of order $1/P$ (namely u_∞/P and c_0/P). Global mass conservation ensures that their sum is finite in the limit $P \to 0$ and we show in appendix B that it is given by

$$\frac{u_\infty + \delta + \eta - 1}{P} = \int_0^1 \mathrm{d}y\, (1 + \zeta_y \tan\phi) k(x-y) \tilde{u}(x-y). \tag{3.41}$$

Note that this term when added to $b_0/2$ (equation (3.35)) cancels the explicit dependence on $k(x-y)$.

Collecting all terms from I_2 and I_1 we obtain the full similarity equation:

$$\frac{\tilde{u}(x)}{2} = \frac{1}{\pi} \int_{-\infty}^{\infty} \mathrm{d}y\, (1 + \zeta_y \tan\phi) H(x-y) \ln \frac{|y|}{\rho}$$

$$- \int_0^1 \mathrm{d}y\, \Delta\zeta (1 + \zeta_y \tan\phi) H(x-y)$$

$$+ \frac{1}{2} \int_0^1 \mathrm{d}y\, (1 + \zeta_y \tan\phi) \tilde{u}(x-y)$$

$$+ \sum_{n=1}^{\infty} \frac{\sin n\pi x_e}{(n\pi)^2} \cos 2n\pi\left(x - \frac{x_e}{2}\right)$$

$$- \frac{1}{\pi} \tan\phi \int_0^1 \mathrm{d}y\, \zeta_y H(x-y) \ln(2|\sin \pi y|)$$

$$+ \frac{1}{2\pi} \oint_{-\infty}^{\infty} \mathrm{d}y\, \frac{\Delta\zeta + y\zeta_y}{\rho^2} \tilde{u}(x-y)$$

$$- \frac{1}{2} \tan\phi \int_0^1 \mathrm{d}y\, \zeta_y \tilde{u}(x-y). \tag{3.42}$$

As it turns out, there is another cancellation, namely of the last term (stemming from I_{2c}) and the $\tan\phi$ term inside the third term on the right-hand side (stemming from the $b_0/2$ term of I_{1c}). In order to make the parameter dependence explicit, we rewrite (3.42) with $\tilde{u}$ replaced by its representation in terms of interface coordinate

and curvature (2.9). Furthermore, we return to the old integration variable x'. Thus we obtain as final, explicit form of the similarity equation:

$$
\begin{aligned}
-\frac{\epsilon(x)}{2}\left\{\chi\zeta(x)+\psi(x)\sigma\kappa(x)\right\} = &-\int_0^1 \mathrm{d}x'\,\frac{\epsilon(x')}{2}\left\{\chi\zeta(x')+\psi(x')\sigma\kappa(x')\right\} \\
&-\int_0^1 \mathrm{d}x'\,\Delta\zeta(1-\zeta_{x'}\tan\phi)\,H(x') \\
&+\frac{1}{\pi}\int_{-\infty}^{\infty}\mathrm{d}x'\,(1-\zeta_{x'}\tan\phi)\,H(x')\ln\frac{|\Delta x|}{\rho} \\
&+\sum_{n=1}^{\infty}\frac{\sin n\pi x_e}{(n\pi)^2}\cos 2n\pi\left(x-\frac{x_e}{2}\right) \\
&+\frac{1}{\pi}\tan\phi\int_0^1 \mathrm{d}x'\,\zeta_{x'}H(x')\ln(2|\sin\pi\Delta x|) \\
&-\frac{1}{2\pi}\,\Xint=_{-\infty}^{\infty}\mathrm{d}x'\,\frac{\Delta\zeta-\Delta x\zeta_{x'}}{\rho^2}\epsilon(x')\left\{\chi\zeta(x')+\psi(x')\sigma\kappa(x')\right\} \qquad (3.43)
\end{aligned}
$$

For $\phi = 0$, this equation reduces to the similarity equation of axisymmetric growth given previously [12]. In particular, the principal value integral becomes an ordinary improper integral.

In the following section, we will discuss some consequences of the full equation.

4. *Consequences of similarity—scaling laws*

The numerical method to solve the boundary integral equation (2.15) has been described in some detail in [12, 16]. We will not repeat that description here but simply discuss the results. For simplicity, we will assume in the following that there is only one thermal length l_T ($= l_T^\alpha = l_T^\beta$), which does not restrict the general validity of our results. The discussion will be given in dimensionless units; for a detailed explanation of the conversion to physical units see [12]. Suffice it here to say that the time scale is set by the diffusion constant D which we always take equal to 1, while the length scale is determined by specification of the thermal (or any other) length.

The most immediate consequence of the similarity equation is that any dimensionless quantity depends on the two parameters σ and χ only. Therefore, the most direct way to check it consists in a comparison of numerically computed interface profiles, for which some of the model parameters are varied while their combinations σ and χ are kept constant. Figure 4 serves to provide such a comparison on the basis of an integration of the full boundary integral equation (2.2).

In the left-hand panel, 17 profiles are displayed which correspond to velocities V between 3.5 and 30.0, while σ and all other parameters, including the thermal gradient G, are kept fixed. If the selected wavelength in tilted growth conforms with the conventional scaling $\lambda \sim V^{-1/2}$, this will correspond (because σ is proportional to $1/\lambda^2 V$) to the usual situation of an experiment in which simply the pulling speed is altered and all other controllable parameters are held at fixed values.

By contrast, in the right-hand panel the thermal gradient was changed along with the velocity so as to keep χ constant as well. Contrary to all appearance, it is not

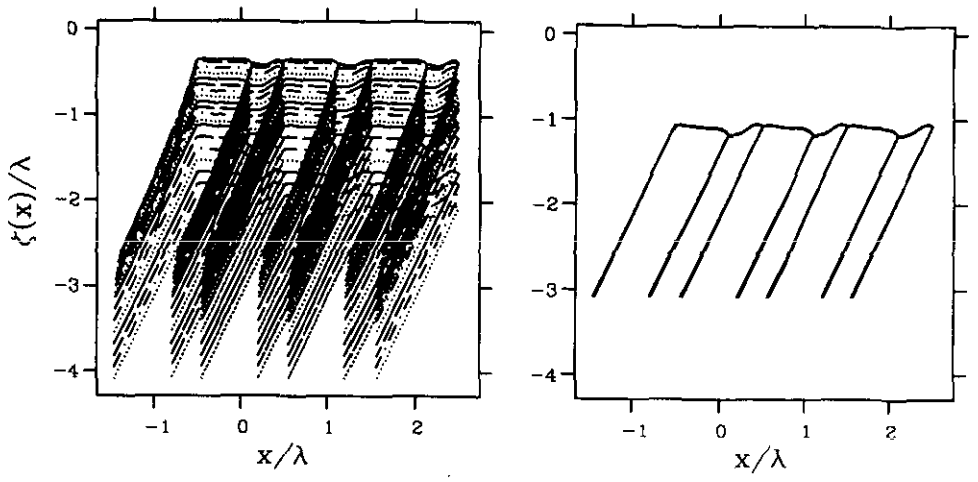

Figure 4. A sequence of numerically calculated interface profiles. The velocities can be read off figures 5–7. The material parameters are: $D = 1$ (sets time scale), $d_0^\alpha = 2 \times 10^{-5}$, $d_0^\beta = 5 \times 10^{-6}$, $k_\alpha = 0.99$, $k_\beta = 1.04$, $u_\infty = 0.05$, $\delta = 0.3$, $\vartheta_\alpha = 0.9 = 51.6°$, $\vartheta_\beta = 0.7 = 40.1°$; $l_T \equiv l_T^\alpha = l_T^\beta$ in both panels of the figure; λ is varied such that $\lambda^2 V$ = constant ($\Rightarrow \sigma$ = constant). On the left-hand side $l_T = 1$, on the right-hand side l_T is varied proportional to l ($\Rightarrow \chi$ = constant).

just one or two profiles which are plotted on the right-hand side of figure 4 but their number is also 17. (That it is larger than 1 may be guessed by careful inspection of the figure, because the line thickness increases towards smaller z values due to slightly different tilt angles.) Amazing as it may seem that so many different profiles covering a rather large velocity range are (almost) identical, this is exactly what is to be expected from the similarity equation. Geometrical identity holds when lengths are measured in units of λ, which means that the true physical patterns are similar to each other with the scale factor given by λ.

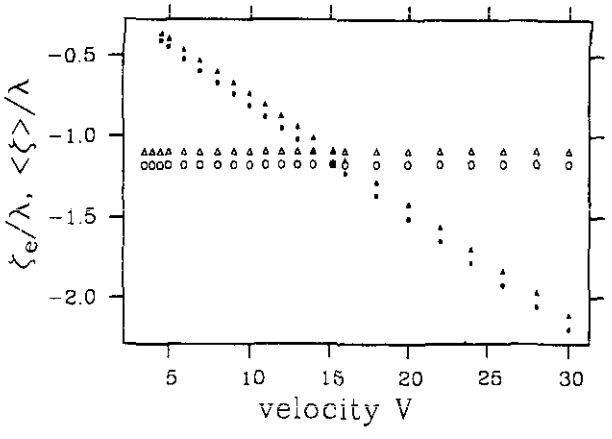

Figure 5. Vertical position of one triple point (the one to the right of the α phase) and average vertical position of the interface as functions of velocity. Triangles: average position; circles: position of triple point. Full symbols: (σ, l_T) = constant (left-hand panel of figure 4); open symbols: (σ, χ) = constant (right panel).

Figures 5 and 6 make the comparison more quantitative. In figure 5, we plot ζ_e, the z coordinate of the eutectic point, as well as $\langle\zeta\rangle = \lambda^{-1}\int dx\, \zeta(x)$, the average z coordinate of the profile, as a function of V. The average undercooling is related to this quantity by $\langle\Delta T\rangle = -G\langle\zeta\rangle$. Whereas for fixed thermal length l_T (i.e. constant gradient G) both reduced quantities show a (strong) linear dependence on the velocity, they remain constant (within our numerical accuracy) in the whole velocity range when σ and χ are kept fixed.

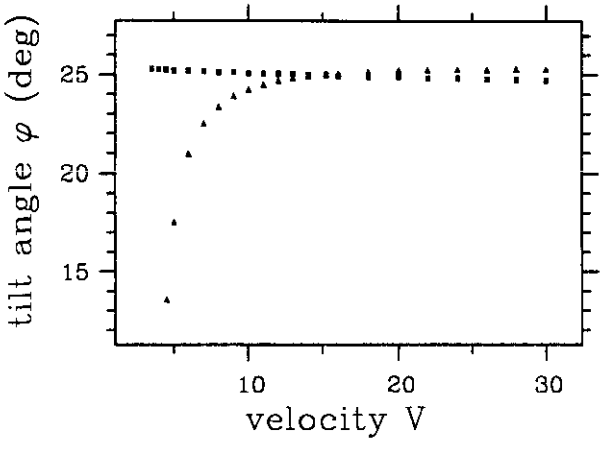

Figure 6. Tilt angle as a function of velocity. The triangles correspond to the left-hand side of figure 4, the squares to the right-hand side.

Figure 5 yields, on a quantitative level, the relative displacement of the profiles given in figure 4, with respect to each other. In figure 6 we investigate the change of the tilt angle along the sequence. Here we do not have to go to reduced quantities, since the tilt angle is dimensionless by itself. Again the numerics confirm our expectations from the similarity equation: with constant σ and χ the tilt angle remains constant under a variation of the velocity, while it decreases with decreasing velocity in the ordinary experimental situation.

This result is well suited for experimental verification. Here, χ is essentially determined by the ratio of G and V; both quantities can be easily controlled in experiments, thus keeping χ fixed while varying V does not pose a specific challenge. Proposing this experiment, we predict ϕ to remain constant over a wide range of growth velocities. Especially at small velocities, the different outcomes of the two experimental protocols corresponding to the left- and right-hand panels of figure 4 should be easily distinguishable.

The final geometric quantity that we consider is the lateral position x'_e of one of the eutectic points (figure 7). (Note that the coordinate system in the numerics is such that x'_e is related to x_e of equation (3.37) via $x'_e/\lambda = x_e - \frac{1}{2}$.) Here we cannot really claim for either of the two cases that there is no variation under velocity change, because even though the total variation is smaller than 3% in the second case, a clear systematic trend is visible—we have a roughly linear (albeit weak) dependence of x'_e/λ on the velocity. This can be understood as follows. The similarity equation (3.43) is the exact $P \to 0$ limit of the integral equation (2.15). For non-zero P, global mass conservation (3.41) requires a (weak) dependence of η and hence of x_e

and x_e' on P—which must of course be seen in any exact numerical solution of the problem. It can be reintroduced (or kept) in the similarity equation by taking into account equations (3.37) and (3.41) in the determination of x_e. This quantity appears not only explicitly in the similarity equation but is also hidden in the integration boundaries because the integrands differ in the different phases (see the discussion of equations (2.9)–(2.14)). The influence of this first-order effect in P can be safely neglected for most quantities because the parameter dependence of η is very weak. However, since x_e is very closely related to η (in the limit of vanishing tilt angle, they are equal), the residual P dependence and the ensuing velocity dependence show up more strongly in this quantity than in others. But the dependence on the velocity is much weaker than for the ordinary experimental situation of constant σ and l_T.

Even more interesting than geometric similarity properties of the growing crystal are new scaling relations that follow from similarity. We have already shown previously for axisymmetric growth [12] that any wavelength selection mechanism, no matter how it operates, leads to a relation between χ and σ which can, without restriction of generality, be cast into the form

$$\lambda \sim \sqrt{d_0 l}\, f\left(\frac{l}{l_T}\right) \tag{4.1}$$

or

$$\lambda \sim V^{-1/2}\, g\left(\frac{G}{V}\right). \tag{4.2}$$

Of course, this result carries over to the non-axisymmetric case without any change. That is, whatever the selection criterion in *tilted* growth (about which there is little experimental information), at constant ratio G/V the selected wavelength will be proportional to $V^{-1/2}$ because of equation (4.2)—and therefore σ has to be constant in the proposed experiment on the tilt angle as soon as χ is fixed. The scaling function g may of course be different from the one we determined for axisymmetric growth [12]. This issue will be taken up again below.

Furthermore, similarity tells us that the tilt angle depends on two relevant parameters only, $\phi = \phi(\sigma, \chi)$, and from the bifurcation diagram [16] we know that, for non-zero ϕ, the value of ϕ determines the wavelength at given velocity and vice versa. Fixing ϕ we therefore obtain, by virtue of the theorem on implicit functions, a functional relation between σ and χ which again takes the form of equation (4.1) or (4.2) (for $\phi = 0$, the derivative of $\phi(\sigma, \chi)$ with respect to either of its arguments becomes zero, rendering the theorem inapplicable). Let us apply equation (4.1) to this case as follows:

$$\lambda_\Phi \sim \sqrt{d_0 l}\, f_\Phi\left(\frac{l}{l_T}\right) \tag{4.3}$$

where the subscript Φ denotes the fixed value of ϕ.

The question arises then whether the scaling function f is universal in the sense that it is the same, up to a constant factor, for different distinguished wavelengths. As an example, we can compare the scaling function obtained for the minimum undercooling wavelength [12] (of axisymmetric solutions) with f_Φ for any desired angle Φ. This comparison is performed in figure 8. In the vicinity of the critical

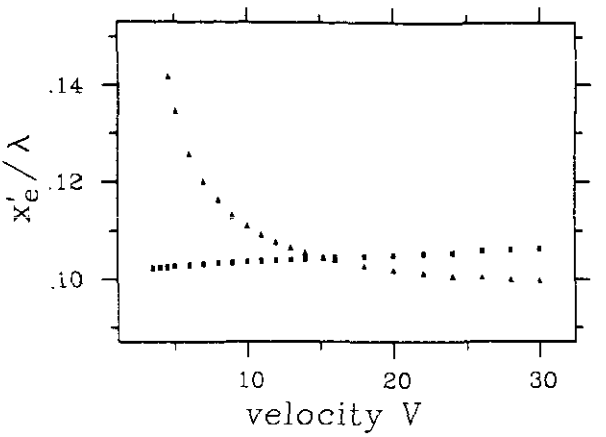

Figure 7. Lateral coordinate of the triple point on the right side of the α phase (the coordinate of the left triple point is fixed to -0.5λ) as a function of velocity. The triangles correspond to the left-hand side of figure 4, the squares to the right-hand side. At the point of intersection $l_T = 1.0$.

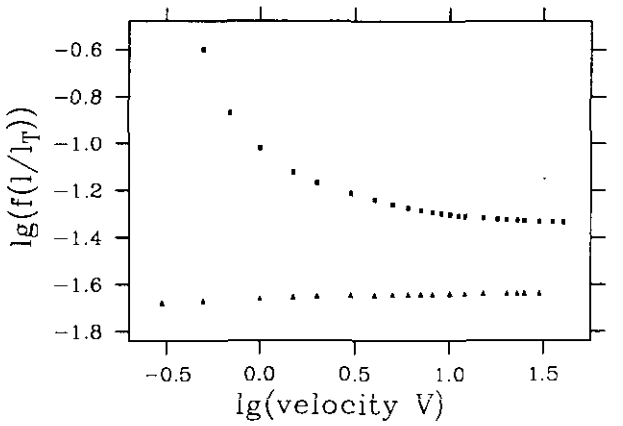

Figure 8. Scaling function $f(l/l_T) = \lambda V^{1/2}$ as a function of the velocity in double logarithmic representation. Squares: $\lambda = \lambda_{0.1}$ (see text); triangles: $\lambda = \lambda_{min}$. The triangles correspond to axisymmetric patterns (the data are identical to that of figure 14 in [12]). For both curves, the velocity is prescribed and λ is calculated, either from the condition $\phi = 0.1$ or from the requirement that the average undercooling be minimum. Material parameters: $d_0^\alpha = d_0^\beta = 10^{-5}$, $l_T^\alpha = l_T^\beta = 1$, rest as in figure 4.

wavelength λ_c of the parity-breaking transition the tilt angle increases strongly with increasing wavelength [16] (the bifurcation is said to be very stiff), so our choice of a rather small angle $\Phi = 0.1$ ($\approx 5.7°$) means that λ_Φ is close to λ_c. Numerically, it is much simpler to scan a sequence of solutions with a fixed tilt angle than directly to determine the critical point. An accurate calculation of the latter would require the computation of a sufficiently large set of profiles with decreasing tilt angle, while the former calculation can be done with one profile per data point by a simple change of the variables for which the Newton iteration scheme [16] is trying to solve, for example by taking λ as a variable instead of ϕ.

The figure shows the non-universality of the scaling function f. Indeed, while $f_{0.1}$ (and any f_Φ) is increasing for decreasing velocity, the scaling function for the minimum undercooling wavelength, let us call it $f_{\min}$, is decreasing. Whereas we do not have any deeper insight in the behaviour of $f_{\min}$ (which is, however, in agreement with experiments [16]), it is quite easy to understand the dependence of f_Φ on V. We know that the tilt angle is constant, if $\sigma = 2d_0^\alpha D/\lambda^2 V$ and $\chi = l/l_T^\alpha$ are kept constant. If we now start with $\phi = \Phi$ at a high velocity and decrease V (i.e. increase l) while keeping σ and l_T constant, the corresponding change of $f_\Phi(\chi)$ is equivalent to one obtained by keeping l constant and decreasing l_T (or increasing the thermal gradient G). But to increase the temperature gradient means to counteract the tilt of the pattern, i.e. the tilt angle should decrease. (It is known that there are no tilted solutions for large thermal gradients [25].) This decrease in turn can be redressed (at fixed velocity) by an increase in λ. But then we can keep ϕ constant (at fixed l_T) by simultaneously decreasing V and increasing λ such that $\lambda^2 V$ increases (because λ must be larger than for constant σ), which means that f_Φ has to increase. No simple arguments of this kind are available for the bottom curve of figure 8.

For the ratio $f_{0.1}/f_{\min}$, which is identical to the ratio of the corresponding wavelengths, we obtain $\lambda_{0.1}/\lambda_{\min} \approx 2.0$ at large velocities ($V \approx 30$), while for $V < 1$ we have $\lambda_{0.1}/\lambda_{\min} \gtrsim 4.3$ and the ratio already exceeds 11.8 at $V = 0.5$.

We suggested previously that an experimental procedure to obtain extended domains of parity-broken states would be to apply a sudden velocity jump by a factor of the order of 4, because then the temporary wavelength after the jump would be by a factor of ≈ 2 larger than the selected wavelength of a symmetric pattern (corresponding to the final velocity) and hence a tilted state would easily form. Our present result shows that this holds quantitatively only if the final velocity is large enough. If we were to try and produce tilted solutions at parameters corresponding to figure 8 and a final velocity of 1, we would need a factor of 4 in wavelength, i.e. an initial velocity which is smaller by a factor of 16! It is easy to imagine that with factors of this order (and beyond) the limits of experimental feasibility will soon be reached. Nevertheless, because $\lambda_{0.1}$ is close to the critical wavelength λ_c for the appearance of tilted solutions, this type of experiment would seem suitable for constructing an estimate for the top curve in figure 8, which is probably not directly accessible in experiments.

In fact, while the bottom curve of figure 8 can be measured with little difficulty (as long as the minimum undercooling criterion gives a good approximation to the selected wavelength), the only way to fix the tilt angle experimentally seems to be to exploit the similarity equation. But then the experiment would be run with $\lambda^2 V$ = constant and G/V =constant, which is not along the top curve of figure 8 (since f which is essentially $\sigma^{-1/2}$ is not constant). In view of the fact that the selection criterion for the tilt angle is unknown (for a conjecture see [16]), it is not clear (and seems rather unlikely) that it is possible to follow that curve 'adiabatically'. As to the numerics, the situation is the reverse: it is much harder to compute the bottom curve than the top one.

In spite of these restrictions it should be possible to check the general statement experimentally: the ratio of the critical wavelength for the tilting instability and the selected wavelength of an axisymmetric pattern at the same velocity should increase with decreasing velocity.

Note that it seems likely from these considerations that the scaling function for the selected wavelength in tilted growth also differs from that for the selected wavelength

in untilted growth, although we have not proved this. We did not try to calculate that scaling function; for apart from our conjecture in [16] we have no clue what the selection criterion might look like and so any determination of the scaling function would have to be based on mere speculation. However, if that scaling function were simply proportional to $f_{\min}$, the selected tilt angle at high velocities would become extremely large. Indeed, the wavelength of a selected state with non-zero angle at low velocities would have to be larger than λ_c; since the scaling function for λ_c decreases with increasing velocity, while that for the selected wavelength was assumed to increase (because of the supposed proportionality to $f_{\min}$), the ratio of selected and critical wavelength would have to increase with increasing velocity; depending on the velocity threshold (if any) above which a tilted solution exists it could easily exceed 10 (see figure 8). Factors of this order would lead to large selected tilt angles (close to 90°), for which there is no experimental evidence.

5. Conclusions

The main result of this paper is the constructive theoretical proof (by its derivation) that there is a similarity equation in lamellar eutectic growth, whether or not the basic stationary patterns are symmetric. This was not clear to begin with since our previous derivation needed the symmetry property.

A first step in deriving a similarity equation for non-symmetric patterns was to see whether the limit $P \to 0$ could be performed despite the apparent divergence of one of the considered integrals; in a second step it had to be recognized that the mathematical structure of the problem did not allow negligence in questions of uniform convergence. Carelessness would be penalized by the loss of terms that are needed in the final equation to cancel other terms. Since the necessity for this kind of mathematical rigour is rarely met in physics, this is an interesting feature in itself.

The form of the new similarity equation is considerably more complex than that of the old one. For $\phi = 0$, the old equation is recovered.

The existence of a similarity equation for general stationary patterns provides the theoretical foundation of our earlier discovery [11, 16] that exact numerical solutions of the basic integral equation (2.2) exhibit similarity properties for tilted patterns as well as for untilted ones.

We suggest two experiments to verify the consequences predicted by the similarity equation:

(i) to monitor the tilt angle as a function of the velocity while keeping σ and χ constant;

(ii) to produce, for a series of different velocities, tilted patterns invading the whole sample by applying sufficiently large velocity jumps, and thus to determine upper bounds for the ratio of the critical wavelength of the tilted pattern and the selected wavelength (at the final velocity) of the underlying symmetric pattern.

The first experiment would check the prediction of constant tilt angle [11, 16] under the described conditions. The second experiment would check the new prediction (not made previously) that the discussed wavelength ratio increases with decreasing velocity and hence the scaling function is non-universal.

Finally, we mention that even the behaviour of the selected wavelength in tilted growth can be predicted for a constant ratio of the thermal gradient and the velocity and that an experimental determination of the corresponding scaling function would

constitute an important step towards a theoretical understanding of the selection criterion.

Appendix A. Convergence considerations

To show the uniform convergence of I_{2a} and I_{2b} we use the representation ([26], no 8.432,9)

$$K_1(xz) = \frac{x}{z}\int_0^\infty \mathrm{d}t\, t^2 \frac{\exp\{-x\sqrt{t^2+z^2}\}}{\sqrt{t^2+z^2}} \tag{A.1}$$

with $x = \rho$ or $x = |y|$ and $z = \tilde{P}$.

Noting that

$$\sqrt{t^2+\tilde{P}^2} \geqslant |\tan\phi|\, P + \left(1 - \frac{|\tan\phi|}{\sqrt{1+\tan^2\phi}}\right) t = \left|\hat{P}\right| + \mu t \tag{A.2}$$

where obviously $0 < \mu \leqslant 1$ for all allowed values of ϕ, we can estimate an upper bound for the factor outside the brackets in the integrand of expression (3.9), defining I_2,

$$\begin{aligned}\left|\tilde{P}\mathrm{e}^{-\hat{P}y}\frac{K_1(P\rho)}{\rho}\right| &= \left|\int_0^\infty \mathrm{d}t\, t^2 \frac{\exp\left\{-\hat{P}y - \rho\sqrt{t^2+\tilde{P}^2}\right\}}{\sqrt{t^2+\tilde{P}^2}}\right| \\ &\leqslant \int_0^\infty \mathrm{d}t\, t\, \mathrm{e}^{-\mu\rho t} = \frac{1}{\mu^2\rho^2}.\end{aligned} \tag{A.3}$$

Furthermore, we will need

$$\begin{aligned}&\left|\frac{\partial}{\partial y}\tilde{P}\mathrm{e}^{-\hat{P}y}\frac{K_1(P\rho)}{\rho}\right| \\ &\quad= \left|\int_0^\infty \mathrm{d}t\, t^2\left(-\hat{P} - \frac{y-\Delta\zeta\zeta_y}{\rho}\sqrt{t^2+\tilde{P}^2}\right)\frac{\exp\left\{-\hat{P}y-\rho\sqrt{t^2+\tilde{P}^2}\right\}}{\sqrt{t^2+\tilde{P}^2}}\right| \\ &\quad\underset{\hat{P}<\tilde{P}}{\leqslant} \int_0^\infty \mathrm{d}t\, t^2\left(1+\frac{|y-\Delta\zeta\zeta_y|}{\rho}\right)\mathrm{e}^{-\mu\rho t} \\ &\quad= \left(1+\frac{|y-\Delta\zeta\zeta_y|}{\rho}\right)\frac{2}{\mu^3\rho^3}.\end{aligned} \tag{A.4}$$

We then split I_{2a} according to

$$\begin{aligned}I_{2a} &= I_{2a}^{(1)} + I_{2a}^{(0)} + I_{2a}^{(2)} \\ &= \int_{-\infty}^{-R_1}\mathrm{d}y\cdots + \int_{-R_1}^{R_2}\mathrm{d}y\cdots + \int_{R_2}^{\infty}\mathrm{d}y\cdots.\end{aligned} \tag{A.5}$$

Clearly, we need to consider $I_{2a}^{(1)}$ and $I_{2a}^{(2)}$ only to show the uniform convergence, and since the case of negative y is the most dangerous situation, we look at $I_{2a}^{(1)}$ explicitly. Introducing

$$G_P(y) = \int_{-R_1}^{y} \mathrm{d}t(g_P(t) - \bar{g}_P) \tag{A.6}$$

we can write

$$I_{2a}^{(1)} = \int_{-\infty}^{-R_1} \mathrm{d}y\, F_P(y)\tilde{P}\mathrm{e}^{-\hat{P}y}\frac{K_1(\tilde{P}\rho)}{\rho} + G_P(y)y\tilde{P}\mathrm{e}^{-\hat{P}y}\frac{K_1(\tilde{P}\rho)}{\rho}\Bigg|_{-\infty}^{-R_1}$$
$$- \int_{-\infty}^{-R_1} \mathrm{d}y\, G_P(y)\left(1 + y\frac{\partial}{\partial y}\right)\tilde{P}\mathrm{e}^{-\hat{P}y}\frac{K_1(\tilde{P}\rho)}{\rho} \tag{A.7}$$

where we have performed an integration by parts. Because $\bar{g}_P$ is the average of $g_P(t)$ over one period, the integral of $g_P(t) - \bar{g}_P$ over one period vanishes. This means that $G_P(y)$ is a bounded function $\forall y \in \mathbb{R}$. Hence the second summand of (A.7) is zero ($G_P(-R_1) = 0$) and using (A.3) and (A.4) we get

$$\left|I_{2a}^{(1)}\right| \leqslant \int_{-\infty}^{-R_1} \mathrm{d}y \left\{|F_P(y) - G_P(y)| + \left|\frac{2y}{\mu\rho}\left(1 + \frac{|y - \Delta\zeta\zeta_y|}{\rho}\right)G_P(y)\right|\right\}\frac{1}{\mu^2\rho^2}. \tag{A.8}$$

The quantity in braces inside the integral is a bounded function ($F_P(y)$ is periodic and $\Delta\zeta$ is also bounded), with an upper bound that can be chosen independent of P for $P \in [0, P_0]$ (the bound may depend on P_0). Since the integral of $1/\rho^2$ is convergent at infinity, this shows the uniform convergence of I_{2a} at the lower integration bound ($-\infty$). An entirely analogous proof can be given for the upper bound, which completes the demonstration of uniform convergence for I_{2a}.

Next we consider I_{2b}. Here we use the inequalities (A.2) and

$$1 - \mathrm{e}^{-x} \leqslant x \qquad \forall x \in \mathbb{R} \tag{A.9}$$

in the following estimate

$$\left|\tilde{P}\mathrm{e}^{-\hat{P}y}\left(\frac{K_1(\tilde{P}\rho)}{\rho} - \frac{K_1(\tilde{P}|y|)}{|y|}\right)\right|$$
$$= \left|\int_0^\infty \mathrm{d}t\, t^2 \frac{\mathrm{e}^{-\hat{P}y}}{\sqrt{t^2 + \tilde{P}^2}}\right.$$
$$\left. - \left(\exp\left\{-\rho\sqrt{t^2 + \tilde{P}^2}\right\}\exp\left\{-|y|\sqrt{t^2 + \tilde{P}^2}\right\}\right)\right|$$
$$= \int_0^\infty \mathrm{d}t\, t^2 \frac{\exp\left\{-\hat{P}y - |y|\sqrt{t^2 + \tilde{P}^2}\right\}}{\sqrt{t^2 + \tilde{P}^2}}$$

$$\times \left(1 - \exp\left\{-(\rho - |y|)\sqrt{t^2 + \tilde{P}^2}\right\}\right)$$

$$\leqslant \int_0^\infty \mathrm{d}t\, t^2 \frac{\mathrm{e}^{-\mu|y|t}}{\sqrt{t^2 + \tilde{P}^2}}(\rho - |y|)\sqrt{t^2 + \tilde{P}^2}$$

$$= (\rho - |y|)\frac{1}{\mu^2\rho^2} = \frac{\rho^2 - y^2}{\rho + |y|}\frac{1}{\mu^2\rho^2} = \frac{\Delta\zeta^2}{\rho + |y|}\frac{1}{\mu^2\rho^2} \tag{A.10}$$

which shows that, for large $|y|$, the factor in I_{2b} that multiplies $y\bar{g}_P$ is of order $1/|y|^3$. Hence the integrand can again be estimated uniformly by a constant times $1/y^2$ for large arguments and the proof of uniform convergence is straightforward.

A convenient way to calculate I_{2c} is to use the integral

$$I_{K1}(\alpha, b, z) \equiv \int_{-\infty}^{\infty} \mathrm{d}x\, \mathrm{e}^{bx} \frac{K_1\left(\alpha\sqrt{x^2 + z^2}\right)}{\sqrt{x^2 + z^2}} = \frac{\pi}{\alpha|z|}\exp\left[-\sqrt{\alpha^2 - b^2}\,|z|\right] \tag{A.11}$$

which leads to

$$\int_{-\infty}^{\infty} \mathrm{d}x\, \mathrm{e}^{bx} \frac{x K_1(\alpha|x|)}{|x|} = \lim_{z\to 0}\frac{\partial}{\partial b} I_{K1}(\alpha, b, z) = \frac{\pi b}{\alpha\sqrt{\alpha^2 - b^2}} \tag{A.12}$$

valid for $\alpha > \Re(b)$. This is formula (3.15), which allows direct evaluation of I_{2c}. The integral (A.11) was previously derived by ourselves in the context of the sum rule for tilted growth [16]. Since this derivation is somewhat tedious, it shall not be reproduced here. Instead (to make this paper self-contained) we outline an alternative approach that the reader can check easily. From formula 6.611,9 in [26]

$$\int_0^\infty \mathrm{d}x\, \mathrm{e}^{-bx} K_0(\alpha x) = \frac{\cos^{-1}(b/\alpha)}{\sqrt{\alpha^2 - b^2}} \tag{A.13}$$

(valid for $\Re(\alpha + b) > 0$) and using $\cos^{-1} x + \cos^{-1}(-x) = \pi$ we obtain

$$I_{K0}(\alpha, b) \equiv \int_{-\infty}^{\infty} \mathrm{d}x\, \mathrm{e}^{bx} K_0(\alpha|x|) = \frac{\pi}{\sqrt{\alpha^2 - b^2}}. \tag{A.14}$$

Here we can differentiate with respect to α and integrate on b to find

$$\int_{-\infty}^{\infty} \mathrm{d}x\, (\mathrm{e}^{bx} - 1)\frac{x}{|x|} K_1(\alpha|x|) = \int_0^b \mathrm{d}b' \frac{\partial}{\partial\alpha} I_{K0}(\alpha, b') = \frac{\pi b}{\alpha\sqrt{\alpha^2 - b^2}} \tag{A.15}$$

where we have employed $x/|x| = |x|/x$ for real x. Making the integral on the left-hand side a principal value integral (with the singularity at $x = 0$), we can drop the second summand of the integrand, which is an odd function, and we recover (3.15).

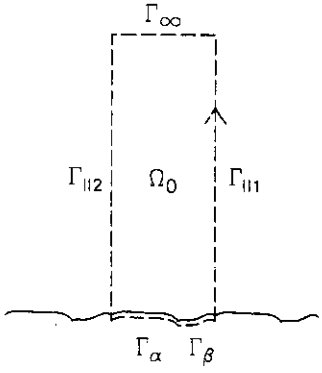

Figure 9. Integration contour used in the derivation of equation (3.41).

Appendix B. Global mass conservation in tilted eutectic growth

In the frame moving with the interface (which for tilted patterns is no longer identical with the laboratory frame), the general form of the continuity equation, valid for both bulk and interface, reads

$$\frac{\partial c}{\partial t} - V\frac{\partial c}{\partial z} - V\tan\phi\frac{\partial c}{\partial x} = -\nabla j_c. \tag{B.1}$$

where j_c is the mass current. In the liquid, where $j_c = -D\nabla c$, the stationary version of this equation reduces to equation (2.1). At the liquid–solid boundary, equation (2.6) may be derived from it.

We now integrate equation (B.1) over the domain Ω_0 delimited by the contour $\Gamma_0 = \Gamma_\alpha + \Gamma_\beta + \Gamma_{\|1} + \Gamma_\infty + \Gamma_{\|2}$ which is depicted in figure 9 and whose bottom pieces Γ_α and Γ_β lie inside the solid. Since we consider stationary solutions, $\partial c/\partial t$ equals zero. The remaining time-independent integrals can be transformed into contour integrals (e_x and e_z denote unit vectors in the x and z directions):

$$\int_{\Omega_0} \mathrm{d}\Omega \left(\frac{\partial c}{\partial z} + \tan\phi\frac{\partial c}{\partial x}\right) = \int_{\Omega_0} \mathrm{d}\Omega\,(e_z + \tan\phi\, e_x)\,\nabla c$$

$$= -\int_{\Gamma_0} \mathrm{d}\Gamma\,(n_z + \tan\phi\, n_x)\,c$$

$$\int_{\Omega_0} \mathrm{d}\Omega\,\nabla j_c = -\int_{\Gamma_0} \mathrm{d}\Gamma\, n j_c. \tag{B.2}$$

The minus sign appears on the right-hand sides, because n is an inward normal with respect to Ω_0. Owing to periodicity, the contributions from $\Gamma_{\|1}$ and $\Gamma_{\|2}$ cancel in both contour integrals.

In the second integral, $j_c = 0$ in the solid as well as at infinity, therefore this integral vanishes altogether (there is no net flux out of the periodicity volume).

The first integral can be transformed into a sum of two integrals on the interval $[0, \lambda]$, with $\mathrm{d}x = n_z\mathrm{d}\Gamma$ for Γ_α and Γ_β and $\mathrm{d}x = -n_z\mathrm{d}\Gamma$ for Γ_∞, where in addition $n_x = 0$. Hence, we obtain in units reduced by λ

$$c_\infty = \int_0^{x_e} \mathrm{d}x\,(1 - \zeta_x\tan\phi)c_{s\alpha}(x, \zeta(x)) + \int_{x_e}^1 \mathrm{d}x\,(1 - \zeta_x\tan\phi)c_{s\beta}(x, \zeta(x)) \tag{B.3}$$

where $c_{s\alpha}$ and $c_{s\beta}$ stand for the concentrations in the α and β phases respectively.

Subtracting c_e on both sides of the equation and subtracting and adding certain integrals containing c_α and c_β on the right-hand side, we arrive at

$$\begin{aligned} c_\infty - c_e = &\int_0^{x_e} dx\,(1-\zeta_x \tan\phi)(c_{s\alpha}-c_\alpha) + \int_{x_e}^{1} dx\,(1-\zeta_x\tan\phi)(c_{s\beta}-c_\beta) \\ &- c_e + \{x_e - \tan\phi\,[\zeta(x_e)-\zeta(0)]\}\,c_\alpha \\ &+ \{1-x_e-\tan\phi\,[\zeta(1)-\zeta(x_e)]\}\,c_\beta \end{aligned} \tag{B.4}$$

which on division by Δc becomes

$$\begin{aligned} u_\infty = &\int_0^{x_e} dx\,(1-\zeta_x\tan\phi)u_{s\alpha} + \int_{x_e}^{1} dx\,(1-\zeta_x\tan\phi)u_{s\beta} \\ &+ \frac{1}{\Delta c}\{x_e(c_\alpha - c_e) + (1-x_e)(c_\beta - c_e) \\ &+ (c_\beta - c_\alpha)\tan\phi\,[\zeta(x_e)-\zeta(0)]\} \end{aligned} \tag{B.5}$$

where we have used periodicity ($\zeta(1) = \zeta(0)$) and defined $u_{si} \equiv (c_{si} - c_i)/\Delta c$ ($i = \alpha, \beta$). An immediate consequence of this definition is $u_{si} = k_i u(x, \zeta(x))$. Furthermore, the brace expression in (B.5) can be simplified to

$$\begin{aligned} &- x_e\delta + (1-x_e)(1-\delta) + \tan\phi\,[\zeta(x_e)-\zeta(0)] \\ &\quad = 1 - x_e - \delta + \tan\phi\,[\zeta(x_e)-\zeta(0)]. \end{aligned} \tag{B.6}$$

Insertion of both results into (B.5) leads to

$$\begin{aligned} u_\infty + x_e + \delta - 1 + \tan\phi\,[\zeta(0)-\zeta(x_e)] &= k_\alpha \int_0^{x_e} dx\,(1-\zeta_x\tan\phi)u(x,\zeta(x)) \\ &+ k_\beta \int_{x_e}^{1} dx\,(1-\zeta_x\tan\phi)u(x,\zeta(x)) \\ &= P\int_0^1 dx\,(1-\zeta_x\tan\phi)k(x)\tilde{u}(x) \end{aligned} \tag{B.7}$$

the definitions of $k(x)$ and $\tilde{u}(x)$ have been given in section 2. Equation (B.7), which is identical to equation (3.41) as we shall see shortly, is the desired result, showing that $(u_\infty + c_0)/P$ does not diverge as $1/P$ but is of order 1 (see equation (3.36)).

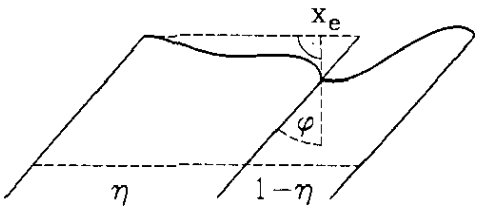

Figure 10. Relation between x_e and the volume fraction η of the α phase (the triple point to the left of the α phase has $x = 0$).

In order to make the connection between x_e and the volume fraction η of the α phase, take a look at figure 10. Obviously, η is given by the length of the segment of a parallel to the x axis cutting through the α phase, since we have normalized the wavelength to one. Here, x_e is not identical with this length whenever the two triple points are not at the same height, i.e. whenever $\zeta(0) \neq \zeta(x_e)$. Now it is elementary geometry to demonstrate from the figure that $\eta = x_e + \tan\phi\,[\zeta(0) - \zeta(x_e)]$, which is identical to equation (3.37). This completes the proof of equation (3.41).

References

[1] Lesoult G 1980 *Ann. Chim. Fr.* **5** 154
[2] Zener C 1946 *Trans. AIME* **167** 550
[3] Brandt W H 1945 *J. Appl. Phys.* **16** 139; 1946 *Trans. AIME* **167**, 405
[4] Jackson K A and Hunt J D 1966 *Trans. AIME* **236** 1129
[5] Langer J S 1980 *Phys. Rev. Lett.* **44** 1023
[6] Datye V and Langer J S 1981 *Phys. Rev.* B **24** 4155
[7] Caroli B, Caroli C and Roulet B 1990 *J. Physique* **51** 1865
[8] Brattkus K and Misbah C 1990 *Phys. Rev. Lett.* **64** 1935
[9] Kassner K and Misbah C 1992 in preparation
[10] Trivedi R, Mason J T and Kurz W 1988 *Acta. Metall.* **19A** 2964
[11] Kassner K and Misbah C 1991 *Phys. Rev. Lett.* **66** 445
[12] Kassner K and Misbah C 1991 *Phys. Rev.* A **44** 6513
[13] Faivre G, de Cheveigné S, Guthmann C and Kurowski P 1989 *Europhys. Lett.* **9** 779
A similar phenomenon was discovered in directional growth of a nematic crystal:
Simon A J, Bechhoefer J and Libchaber A 1988 *Phys. Rev. Lett.* **61** 2574
[14] Coullet P, Goldstein R and Gunaratne G H 1989 *Phys. Rev. Lett.* **63** 1954
[15] Kassner K and Misbah C 1991 *Phys. Rev. Lett.* **65** 1458 (erratum 1991 **66** 522)
[16] Kassner K and Misbah C 1991 *Phys. Rev.* A **44** 6533
[17] Faivre G, Guthmann C and Mergy J 1991 private communication
[18] Langer J S 1980 *Rev. Mod. Phys.* **52** 1
[19] Abramowitz M and Stegun I A (eds) 1972 *Handbook of Mathematical Functions* (New York: Dover)
[20] Brebbia C A 1978 *The Boundary Element Method for Engineers* (London: Penetech)
[21] Saito Y, Goldbeck-Wood G and Müller-Krumbhaar H 1988 *Phys. Rev.* A **38** 2148
[22] Misbah C 1986 *J. Physique* **47** 1077
[23] Caroli B, Caroli C, Roulet B and Langer J S 1986 *Phys. Rev.* A **33** 442
[24] Bronstein I N and Semendjajew K A 1983 *Taschenbuch der Mathematik* (Thun: Harri Deutsch)
[25] Brattkus K, Caroli B, Caroli C and Roulet B 1990 *J. Physique* **51** 1847
[26] Gradshteyn I S and Ryzhik I M 1980 *Table of Integrals, Series, and Products* (Orlando, FL: Academic)